Cellulose (2021) 28:7053–7073
https://doi.org/10.1007/s10570-021-03958-9

ORIGINAL RESEARCH

Cellulosic bionanocomposites based on acrylonitrile butadiene rubber and *Cuscuta reflexa*: adjusting structure-properties balance for higher performance

Midhun Dominic · Rani Joseph · P. M. Sabura Begum · Athira S. Kumar · P. A. Jeemol · Thomasukutty Jose · Dileep Padmanabhan · Krzysztof Formela · Suchart Siengchin · Jyotishkumar Parameswaranpillai · Mohammad Reza Saeb

Received: 7 January 2021 / Accepted: 15 May 2021 / Published online: 14 June 2021

Abstract Design and manufacture of cellulosic nanocomposites with acceptable performance is in the period of a transition from fantasy to reality. Typically, cellulosic nanofillers reveal poor compatibility with polymer matrices. Thus, adjusting the balance between structure and properties of cellulosic bionanocomposites by careful selection of parent ingredients is the first priority. Herein, we incorporated *Cuscuta reflexa* derived cellulose nanofibers (CNFs) into acrylonitrile-butadiene rubber (NBR) for high-performance elastomeric applications. Tensile and tear strength of NBR improved by $\sim$ 125 and $\sim$ 105 %, respectively at a very low loading of 4 phr CNFs, as a result of interfacial bonding, as evidenced by fractographic analysis. In parallel, the temperature at which maximum degradation occurs (T_{max}) of NBR rose by 14 °C. The swelling index and molar uptake of toluene were also lowered. The Wolff-activity coefficient, hardness, abrasion resistance, and cross-link density were all improved correspondingly. The positive shift in glass transition temperature and the fall in the loss tangent peak height for bionanocomposites proved the effective immobilization of NBR chains by well-dispersed CNFs. The hydrogen bonding interaction between –OH groups of CNFs and –CN groups of NBR might be responsible for the superior performance of NBR/CNF composites, which is confirmed by Fourier transform infrared spectroscopy (FTIR) and X-ray diffraction analysis (XRD).

M. Dominic
Department of Chemistry, Sacred Heart College (Autonomous), Kochi, Kerala 682013, India

M. Dominic (✉) · P. M. S. Begum
Department of Applied Chemistry, Cochin University of Science and Technology (CUSAT), Kochi, Kerala 682022, India
e-mail: midhundominic@shcollege.ac.in

R. Joseph · D. Padmanabhan
Department of Polymer Science and Rubber Technology, Cochin University of Science and Technology (CUSAT), Kochi, Kerala 682022, India

A. S. Kumar
Department of Chemistry, St. Albert's College (Autonomous), Kochi, Kerala 682018, India

P. A. Jeemol
Department of Chemistry, M.E.S. Mampad College, Mampad, Kerala 682018, India

T. Jose
Department of Basic Sciences, Amal Jyothi College of Engineering, Kanjirapally, Kottayam, Kerala 686518, India

K. Formela (✉)
Department of Polymer Technology, Faculty of Chemistry, Gdańsk University of Technology, Gabriela Narutowicza 11/12, 80–233 Gdańsk, Poland
e-mail: krzysztof.formela@pg.edu.pl

Keywords *Cuscuta reflexa* · Cellulose nanofiber · Cross-link density · Glass transition temperature · Thermal stability

Graphic abstract

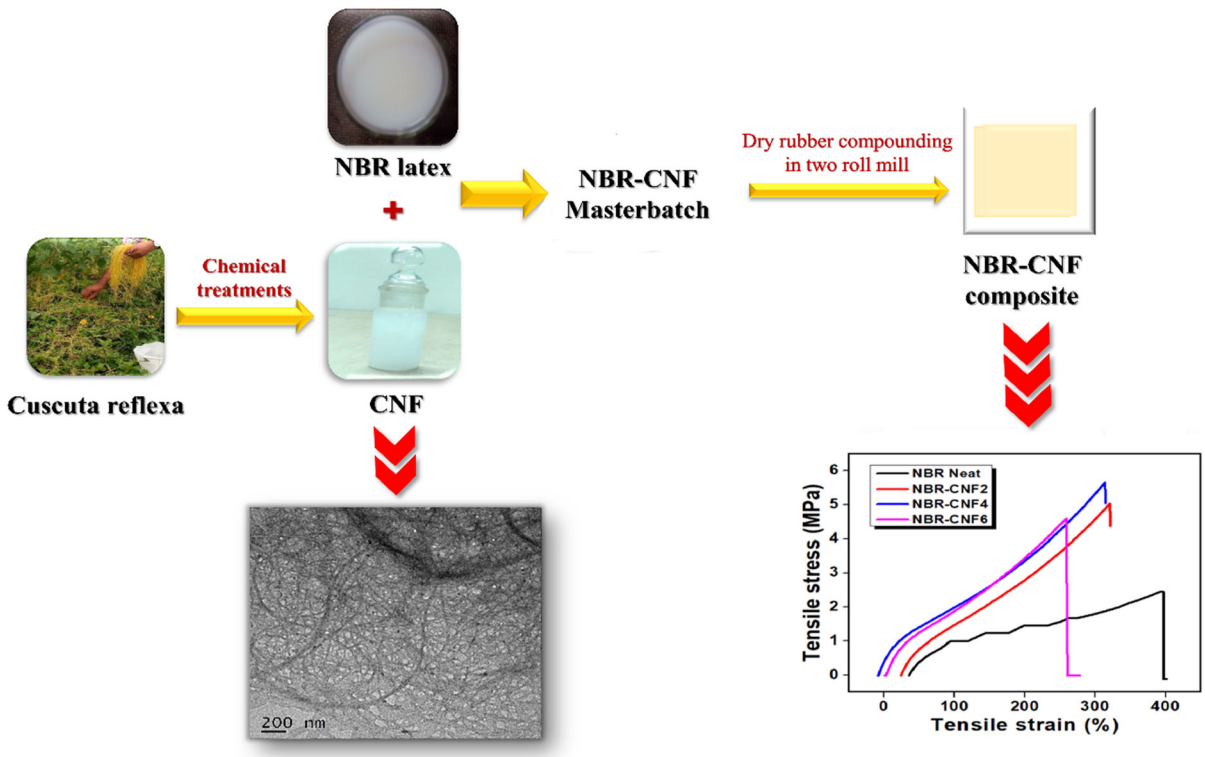

Introduction

Cellulosic polymer nanocomposites are systems in which cellulose-derived nanofillers are incorporated into a polymer with the mission to enhance thermal and mechanical properties (Khattab et al. 2017). Cellulosic nanofibrillar structures have been at the core of attention over the past two decades in view of being plentiful and renewable. The main sources from which cellulose nanofibrils are obtained include in wood, agricultural residues, and bacterial cellulose. Cellulose nanocrystals (CNCs) are known for their biodegradability, relatively high strength, and Young's modulus; therefore, CNCs have been widely utilized in the development of cellulosic nanocomposites (Mariano et al. 2014). Compared to classical

S. Siengchin
Department of Materials and Production Engineering, The Sirindhorn International Thai-German Graduate School of Engineering (TGGS), King Mongkut's University of Technology North Bangkokm (KMUTNB), 1518 Pracharat 1 Road, Wongsawang Road, 10800 Bangsue, Bangkok, Thailand

J. Parameswaranpillai (✉)
School of Biosciences, Mar Athanasios College for Advanced Studies Tiruvalla (MACFAST), Pathanamthitta, Kerala, India
e-mail: jyotishkumarp@gmail.com

M. R. Saeb
Center of Excellence in Electrochemistry, School of Chemistry, College of Science, University of Tehran, Tehran, 14155-6455, Iran

fibers, CNCs have higher aspect ratio, surface area, higher crystallinity, flame retardancy, and thermal stability (Foster et al. 2018). They have elastic modulus (139.5 GPa) and Young's modulus (206 GPa) values more or less equal to those of Kevlar® and steel (Lin and Dufresne 2014). Nevertheless, poor properties of cellulosic nanocomposites are addressed as a consequence of the lack of compatibility between cellulose and plastics (Hubbe et al. 2008). In this sense, CNC modification/functionalization and CNC separation from new sources have attracted widespread interests in academia and industry alike.

There are several reports on the preparation and characterization of elastomer-based nanocomposites reinforced with nanocellulose. A variety of rubbers including natural rubber (NR), styrene-butadiene rubber (SBR), epoxidized natural rubber (ENR), and butadiene rubber (BR) have been reinforced for the thermal, mechanical, barrier, and dynamic mechanical properties (Nunes 2017). Flauzino Neto et al. studied the reinforcing effect of soy hull-derived CNCs in NR and reported that the improvement in the mechanical properties of the composites was greatly influenced by the aspect ratio and percolating network of CNCs (Flauzino Neto et al. 2016). Chen et al. investigated the role of CNCs in the cure behavior, cross-link density, and dynamic mechanical properties of NR/BR/SBR blends (Chen et al. 2014). They observed that CNCs can be used as a green alternative for carbon black (at 10 phr loading) in NR/BR/SBR blend when resorcinol and hexamethylenetetramine (RH) was used to modify the interface. Visakh et al. evaluated the transport properties of cellulosic nanofibers (CNFs) and crystals (CNCs) reinforced natural rubber composites. They observed that the equilibrium solvent uptake and swelling index were found to be minimum for CNF reinforced NR composites rather than CNCs (Visakh et al. 2011).

Acrylonitrile butadiene rubber (NBR) is a polar rubber that enjoys from high compression set, heat resistance, oil resistance, and abrasion resistance (Elsabbagh and Mohamed 2011). In this regard, it has been considered in manufacturing diverse products such as seals, hoses, pipelines, belts, grommets, mats, and gloves (Taib et al. 2017). However, it is not biodegradable and duffers from lack of strain-induced crystallization (Sadeghalvaad et al. 2019a). NBR has been reinforced with CNCs in several studies. Taib et al. improved the tensile strength of NBR from 8.26 to 16.58 MPa (ca. two-fold) by incorporation of 5 phr CNCs (Taib et al. 2020). Cao et al. observed the 'Payne effect' in CNC-reinforced NBR composites (Cao et al. 2013a). They reported that the glass transition temperature (T_g) improved from 10.8 to 17.2 °C with the incorporation of 20 phr CNCs into NBR. Chen et al. reported enhanced modulus at −70 °C of NBR foam from 610 to 1150 MPa (ca. two-fold) by incorporating 15 phr CNCs (Chen et al. 2014). They concluded that the hydrogen bonding between the hydroxyl groups of CNCs and nitrile groups of NBR is responsible for higher performance. There have been also some reports on surface modification of CNCs, e.g. with gallic acid to prepare antioxidant CNC (Aox-CNC) which improved tensile properties, thermal stability, and biodegradability of NBR (Taib et al. 2019). However, in most cases highly loaded cellulosic NBR nanocomposites were prepared, which arises from inadequate properties of CNCs. This highlights the need for finding proper sources of CNCs with high interfacial adhesion to NBR at low loading levels.

The incompatibility between the polar filler and the non-polar matrix is the main reason for poor properties. Surface modification of matrix or filler with suitable surface modifying/coupling agents is a key to improve interfacial adhesion. Acetylation, urethanization, etherification, peptide coupling, esterification, silylation, titanate coupling, polymer grafting, and 2,2,6,6-tetramethylpiperidine-1-oxyl (TEMPO) mediated oxidation are some of the common ways to improve the hydrophobicity of CNFs and thereby enhance the interfacial adhesion between CNFs and the non-polar polymer matrix (Chakrabarty and Teramoto 2018). It is reported that the use of resorcinol-hexamethylenetetramine (RH) could improve the dispersion of CNC in natural rubber (NR) (Jiang and Gu 2020). It is noticed that the rolling resistance of NR/CNC/RH composite was less than that of NR/CNC composite without compromising the wet-skid resistance, which is crucial for developing green tires. CNFs derived from Agave angustifolia can improve the thermal stability and biodegradability of polylactic acid/natural rubber blend when compatibilized with liquid natural rubber (Rosli et al. 2019). Eldho et al. studied the influence of the Zn-cellulose complex and three-dimensional network structure of CNFs in improving the mechanical and dynamic-mechanical properties of natural rubber (Abraham et al. 2013a).

Attachment of –SH or –C = C functional groups to the surface of CNFs by grafting it with suitable surface modifying agents enhanced solvent (toluene) uptake, and rubber damping is greatly decreased by the introduction of grafted CNFs in styrene-butadiene rubber (SBR) (Sinclair et al. 2019). The influence of hydrogen bonding between the filler and the matrix in improving the mechanical properties of the composites was well explained in silica-NBR (Suzuki et al. 2005), cellulose-NBR (Chen et al. 2015), and halloysite nanotube-NBR systems (Ismail and Ahmad 2013).

The use of coupling agents is one of the classical ways to improve the interfacial adhesion between the filler and the polymer. But, the utilization of costly coupling agents (e.g. silane coupling agents) in improving the dispersibility of CNFs in the polymer matrix makes the entire process tedious and uneconomic. Herein, we incorporated the cellulose nanofibers in the NBR latex to prepare a masterbatch so as to enhance the dispersibility and interfacial adhesion between CNFs and the NBR. Then, the masterbatch was compounded with solid NBR and other vulcanizing agents in a two-roll mill to improve the properties of NBR. We make use of hydrogen bonding interaction between the –OH groups of CNFs and –CN groups of NBR as a simple yet smart way to improve the physico-chemical, thermal, mechanical, transport, and dynamic mechanical properties. To the best of the knowledge of the authors of this work, no detailed investigation is available on the impact of the latex coagulation process followed by two rolls milling in processing NBR/CNF composites. The new source of CNFs (*Cuscuta reflexa*) and the lower amount of CNFs (2 to 6 phr) used in this study compared to previous works are features of innovative approach developed. Moreover, there is no detailed investigation on the reinforcing effect of plant-derived CNFs on the NBR. The *Cuscuta reflexa* is a parasitic plant consisting of 100–170 species of yellow, orange, or red parasitic plants mainly found throughout the temperate and tropical regions of the world, and commonly available in Kerala, India in large volume (Paul et al. 2019). In a previous work, we used CNFs with high crystallinity index (67 %) and diameter in the range 10–30 nm extracted from the parasitic plant *Cuscuta reflexa* using steam explosion in presence of 5 % oxalic acid and found it a promising green nanofiller with acceptable compatibility with elastomers (Dominic C.D. et al. 2020a). Herein, NBR/CNF nanocomposites were prepared and characterized for cure behavior, physico-mechanical, thermal, fractographic, viscoelastic, and transport properties. Attempts have been paid to emphasize the significance of the careful selection of cellulosic fibers and elastomer matrix which guarantees adequate interfacial interaction for high-performance applications.

Materials and methods

Materials

The cellulosic nanofibers (10–30 nm) with high crystallinity index (67 %) isolated from *Cuscuta reflexa* were used in this study (Dominic et al. 2020a). The plant possesses a distinct appearance being leafless, rootless, and smooth lacking chlorophyll can parasitize the host through haustoria. Agriculturalists consider them as a destructive weed as it can parasitize multiple adjacent hosts simultaneously which can also affect commercially valuable crops such as flax, alfalfa, bean, and potatoes. The chopped *Cuscuta reflexa* fibers were heated with 2 % NaOH solution to remove hemicellulose and lignin. The alkali-treated fibers were steam-exploded in an autoclave with 5 % oxalic acid to yield CNFs. The detailed procedure for the extraction of CNFs and their characterization are described in our previously reported work (Dominic et al. 2020a). Acrylonitrile-butadiene latex with 34 % acrylonitrile (AN) content was obtained from Eliokem India Pvt. Ltd., Bombay. Acrylonitrile-butadiene rubber (KNB 35 L) with 34 % AN content was purchased from Kumho Petrochemicals Co., Ltd., South Korea. The rubber additives used such as zinc oxide, stearic acid, 1,2-dihydro-2,2,4-trimethyl quinoline (TQ), N-cyclohexyl-2-benzothiazole sulphenamide (CBS), tetramethylthiuram disulphide (TMTD), sulphur, oxalic acid, hydrochloric acid, sodium hydroxide, hydrogen peroxide, and calcium chloride were industrial-grade used without further purification.

Methods

Preparation of NBR/CNF composites

The rubber compounding was done according to ASTM D 3184. The NBR/CNF composites were prepared as follows. First, the masterbatches of NBR latex/CNF were prepared by coagulation using a 0.5 % $CaCl_2$ solution. This was followed by compounding the masterbatches of NBR/CNF latex with solid NBR using a two-roll mill (size 6″ × 12″). The compound was then mixed with vulcanizing agents and other ingredients. Later, the vulcanization was carried out using an electrically heated hydraulic press at 160 °C and a pressure of 2844 psi. The formulations of the prepared NBR/CNF composites are given in Table 1.

Characterization

The rubber process analyzer, RPA 2000 was used to study the cure characteristics of NBR/CNF composites based on ASTM D 5289. The tensile properties and tear resistance of the composites were measured using a universal testing machine (Shimadzu Model AGI) based on ASTMD 412 and ASTM D 624, respectively. Shore A type durometer was used to study the hardness of NBR and NBR/CNF composites based on ASTM D 2240. Bareiss DIN abrader, Germany was used to study the abrasion resistance according to ASTM D 5963. The compression set apparatus was used to study the compression set of the NBR composites according to ASTM D 395. TA instrumentQ-50 thermogravimetric analyzer was used to measure the thermal properties of the composites. The test was carried out in a nitrogen atmosphere at a heating rate of 20 °C /min from 30 to 500 °C. Scanning electron microscope JEOL JSM 8390 LV was used to study the tensile fracture surface of the NBR/CNF composites.

Swelling behavior and cross-link density of the NBR/CNF composites were studied as in our previous publication (Dominic et al. 2020b). The equilibrium swelling method was used to evaluate the swelling behavior of the composites. Toluene was used as the solvent.

The solvent uptake (Q_t), swelling coefficient, and swelling index were measured using the Eqs. 1, 2 and 3:

$$Q_t = \left(\frac{(W_S - W_i)/M_s}{W_i} \right) \times 100\% \quad (1)$$

$$Swelling\ Coefficient = \frac{W_s - W_i}{W_i} \times \rho_s \quad (2)$$

$$Swelling\ Index = \frac{W_s - W_i}{W_i} \quad (3)$$

where W_i and W_s are the weight of the composite samples before and after the swelling studies. M_s and ρ_s are the molar mass and density of the solvent used (toluenē).

The cross-link density (ν) of the nanocomposites was calculated using Eq. (4):

$$v = \frac{1}{2M_c} \quad (4)$$

where M_c is the molecular weight of NBR segments between the cross-links. Based on the Flory-Rehner theory, the M_c is given by Eq. 5 (Flory and Rehner 1943):

Table 1 Formulations for NBR/CNF composites. In this table, formulations are based on 100 parts by weight of NBR and other ingredients are added in part per hundred (phr), i.e. part by weight of additives based on 100 parts by weight of reference NBR

Sample Code	Solid NBR	Masterbatch		ZnO	Stearic acid	TQ	CBS	TMTD	S
		NBR latex	CNF						
NBR -gum	50	50	0	4.5	2	1	1	0.25	2.5
NBR-CNF2	50	50	2	4.5	2	1	1	0.25	2.5
NBR-CNF4	50	50	4	4.5	2	1	1	0.25	2.5
NBR-CNF6	50	50	6	4.5	2	1	1	0.25	2.5

$$M_c = \frac{-\rho_r V_s V_r^{1/3}}{\ln(1 - V_r) + V_r + \chi V_r^2} \quad (5)$$

In this equation ρ_r is the density of the NBR, V_s is the molar volume of toluene, V_r is the volume fraction of swollen NBR and χ is the NBR-toluene interaction parameter (Bryan and G. N. Welding 1964).

The values of V_r and χ were calculated using the Eqs. 6, 7.

$$V_r = \frac{(d - fw)\rho_r^{-1}}{(d - fw)\rho_r^{-1} + A_s\rho_s^{-1}} \quad (6)$$

$$\chi = \beta + \frac{V_s(\delta_s - \delta_p)^2}{RT} \quad (7)$$

In this equation, d is the deswollen weight of the NBR, f is the volume fraction of the insoluble components, w is the initial weight of the NBR, β is the lattice constant, R is the gas constant, T is the absolute temperature, and δ_s and δ_p are the solubility parameter of the toluene and NBR.

TA Instrument DMA Q800 was used to study the viscoelastic properties of the NBR/CNF composites in tension mode from −40 to 80 °C. The sample dimension used for the study was 30 × 3 × 2 mm^3. The composites were tested at a heating rate of 3 °C/min. The frequency used for testing was 1 Hz.

The volume fraction of the NBR chains immobilized because of the filler-polymer interactions was determined from the DMA studies using Eq. 8 (Formela et al. 2016):

$$C_v = 1 - (1 - C_0)\frac{W}{W_0} \quad (8)$$

where $C_v$and C_0 are the volume fraction of the constrained regions in NBR/CNF composites and pure NBR, respectively. The value of C_0 is taken as zero. TheW and $W_0$are the energy loss fraction of CNF reinforced NBR composite and neat NBR. The energy loss fraction was related to *tanδ* by the following Eq. (9):

$$W = \frac{\pi\tan\delta}{\pi\tan\delta + 1} \quad (9)$$

Further, to study the interfacial adhesion between the nanofiber and NBR matrix, the adhesion factor () was evaluated using Eq. 10 (Formela et al. 2016):

$$W = \frac{\pi\tan\delta}{\pi\tan\delta + 1}\frac{\tan\delta_c}{\tan\delta_m} - V_f + A \quad (10)$$

Where *tan* δ_c and *tan* δ_m are the loss tangent of CNF reinforced NBR composites and pure NBR, respectively and V_f is the volume fraction of the CNFs.

Results and discussion

Fourier Transform Infrared (FTIR) analysis

The FTIR analysis was conducted to study the interaction between CNFs and NBR. The FTIR spectra of pure CNFs, pristine NBR and NBR/CNF4 composite are shown in Fig. 1. The functional group analysis of pure CNFs is detailed in our previously reported work (Dominic et al. 2020). The transmission peaks of NBR observed at 2921 − 2846 cm^{-1} which correspond to asymmetric and symmetric –CH vibration (Sadeghalvaad et al. 2019b). The peaks observed at 2237 cm^{-1} and 1719 cm^{-1} in the FTIR spectra of neat NBR correspond to –CN stretching and –C = O stretching vibrations (Abdul Rashid et al. 2018). The peak at 967 cm^{-1} is related to C-H stretching of butadiene double bond (–CH = CH (trans)) and the peak at 690 cm^{-1} corresponds to the RCH = CHR bending vibration (Abdul Rashid et al. 2018). The peaks located at 1440, 1350, 1064 cm^{-1}, and 1540 cm^{-1} in the FTIR spectra of pristine NBR indicate $–CH_2$ bending vibration, $–CH_2$ deformation,

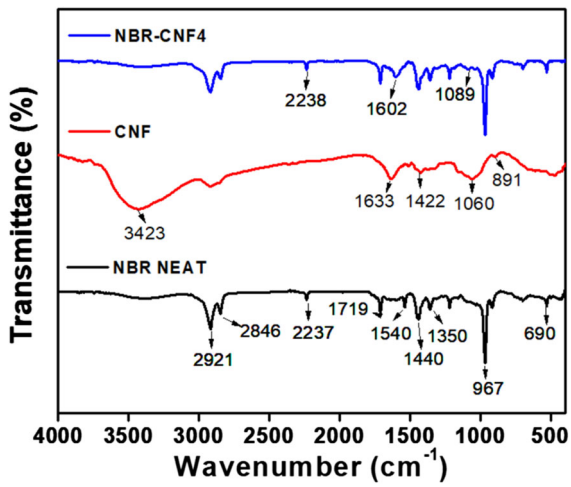

Fig. 1 FTIR spectra of pure CNFs, pristine NBR, and NBR/CNF4 composite

C-O stretching, and -C = C- bond stretching respectively (Ramesan and Nihmath 2017, Abdul Rashid et al. 2018). The increase in the intensity of the peak at 1089 cm^{-1} in the FTIR spectra of the NBR/CNF4 composite confirms the presence of CNFs in the NBR matrix. The peak at 1089 cm^{-1} corresponds to the glycosidic rings of CNF chains (Abdul Rashid et al. 2018). The peak positioned at 2237 cm^{-1} is transit to 2238 cm^{-1} (higher wavenumber region) in the FTIR spectra of NBR/CNF4 composite indicate effective interaction has taken place between the –CN functional groups of NBR and –OH functional groups of CNFs. A similar observation was also made by Sadeghalvaad et al. while studying the interaction between nanoclay, $CaCO_3$ and silica with NBR (Sadeghalvaad et al. 2019b). The shift in the position of the peak from 1540 cm^{-1} to 1602 cm^{-1} in the FTIR spectra of NBR/CNF4 composite also confirms the interfacial interaction between CNFs and NBR.

X-ray diffraction analysis (XRD)

The XRD analysis was performed on pristine NBR and NBR/CNF composites to evaluate the phase purity and fiber-matrix interaction. The XRD pattern of pure CNFs is shown in Fig. 2 A. The XRD analysis of pure CNFs is detailed in our previously reported work (Dominicet al. 2020). Figure 2B showed the XRD patterns of pristine NBR and NBR/CNF composites. The pristine NBR shows a broad peak at $2\theta = 19.47°$ is due to the amorphous nature of the polymer matrix. All the prepared composites also show a broad diffraction peak at around $2\theta = 19°$. The broad diffraction peaks for NBR/CNF2, NBR/CNF4, and NBR/CNF6 composites are observed at 19.15°, 19.07°, and 18.99° respectively. The shift in diffraction peak to lower 2θ values for the composites indicate good interaction between the CNFs and the NBR matrix. On the other hand, the decrease in the breadth of the peaks in the composite samples indicate a reduction in the amorphous nature of the NBR polymer. Ramesan and Nihmath observed a similar shift in 2θ values and a decrease in the breadth of the main peak in NBR-hydroxyapatite nanocomposites (Ramesan and Nihmath 2017). Apart from the broad diffraction peak centered at around $2\theta = 19°$, a shoulder peak at $2\theta = 22.27°$ is observed in all NBR/CNF composites. The peak at $2\theta = 22.27°$ is the characteristic crystalline diffraction peak from the (200) plane of cellulose nanofibers (Bahloul et al. 2021). This peak is not observed in the XRD pattern of pristine NBR. The presence of the shoulder peak at $2\theta = 22.27°$ in NBR/CNF composites confirms the successful incorporation of CNFs in to the NBR matrix.

Cure characteristics of NBR/CNF composites

Table 2 exhibits the cure characteristics of CNF reinforced NBR composites. The optimum cure time is the time required to reach 90 % of the maximum torque and the values of optimum cure time of NBR/CNF composites are observed to be higher than NBR. The interaction of the hydroxyl groups of cellulosic nanofibers with accelerators and activators may reduce the number of active curing agents required for vulcanization. That might be the reason for the increase in cure time for the prepared NBR/CNF nanocomposites. Rajkumar et al. also reported an increase in cure time when silica particles are used as a reinforcing filler in NBR (Rajkumar et al. 2013). Scorch time is the time required for the onset of vulcanization, or in other words, it gives information on the processing safety of the prepared nanocomposites. It was observed that scorch time increases with an increase in CNF loading. Thus, the addition of CNFs into the NBR matrix improves the scorch safety of the prepared NBR-CNF nanocomposites. The cure rate index (CRI) of the prepared nanocomposites is found to be decreasing with an increase in CNF content. Among the nanocomposites prepared, NBR/CNF4 shows the highest CRI value. The low cure rate index makes the processability of the composite difficult. The decrease in the CRI of NBR/CNF composites was probably due to the restricted movement of free radicals generated during vulcanization by the surface functionalities (hydroxyl groups) of CNFs (Kulshrestha et al. 2020). Thus, the cellulosic nanofibers have a negative effect on the cure reaction of NBR. The minimum torque provides information on the viscosity of the material and is higher for the prepared NBR-CNF nanocomposites compared to pristine NBR. The maximum torque which is an indication of the shear modulus of the material was found to be maximum for NBR/CNF4 composite. The increase in the maximum torque values of NBR/CNF composites

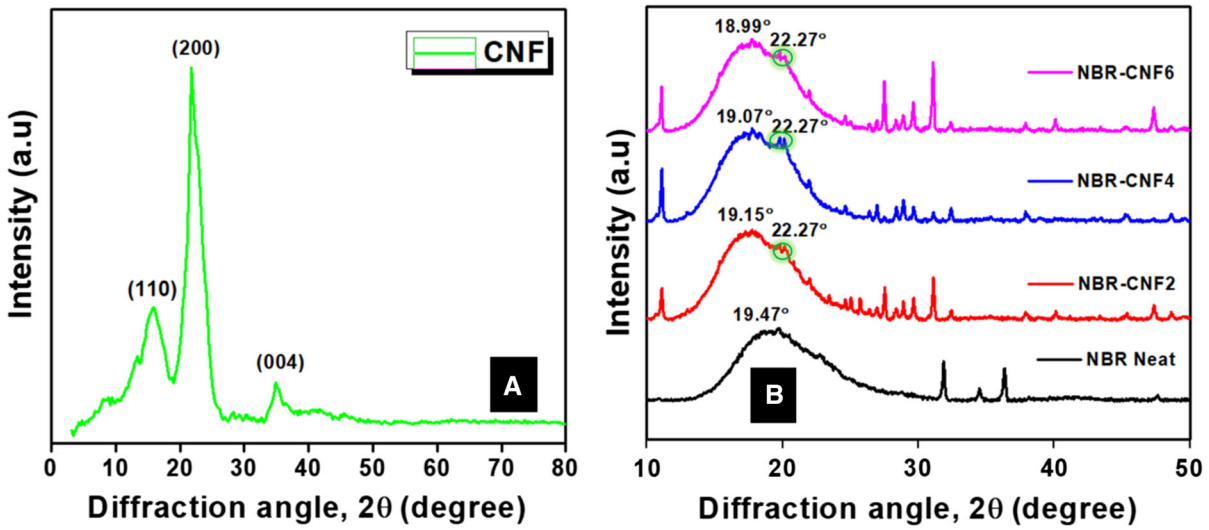

Fig. 2 **a** Diffraction patterns of pure CNFs **b** pristine NBR and NBR/CNF composites

Table 2 Curing parameters and Wolff activity coefficient determined for NBR/CNF nanocomposites

Properties	NBR- gum	NBR/CNF2	NBR/CNF4	NBR/CNF6
Scorch time, t_{s2}(min)	1.28	1.39	1.30	1.35
Optimum cure time, t_{90}(min)	2.56	4.46	3.25	4.12
Cure rate index (min^{-1})	78.12	32.57	51.28	36.10
Minimum torque(M_L, dNm)	0.43	0.46	0.47	0.49
Maximum torque(M_H, dNm)	2.51	2.66	2.73	2.60
Differential torque, $M_H - M_L$ (dNm)	2.08	2.20	2.26	2.11
Wolff activity coefficient	–	2.88	2.16	0.24

is an evidence of the confinement of the polymer chains and reduced macromolecular mobility. The values of maximum torque is dependent on the cross-link density and fiber-matrix interaction (Visakh et al. 2012b). The maximum torque for NBR/CNF4 composite shows better entanglement of rubber chains with CNFs. At high CNF loading, the agglomeration of nanofibers results in poor wetting of the fibers with polymer chains. This is the reason for the decrease in the maximum torque at higher filler loading.

The activity of CNFs in NBR can be monitored by the change in torque moment when the sample is cured in an oscillatory rheometer. The Wolff activity coefficient (α_F) gives information on the reinforcing effect of filler in the matrix. Studies have shown that the composites with a higher valueof α_F shows better reinforcing effect (Formela et al. 2016). Wolff activity coefficient depends on the parameters ΔM_x (the torque increment of NBR/CNF composites) and ΔM_0 (torque of NBR), m_x (the weight of CNFs) and m_p (the weight of NBR matrix). The value α_F gives information on the effect of reinforcement of the fibers in the NBR matrix. The negative value showed no reinforcement, while the positive value showed good reinforcement. The value of α_F depends on the total composition of the rubber compound, type of the rubber, nature of the filler and the curing system (Kruželák et al. 2015).The α_F can be calculated from the following Eq. (11):

$$\frac{\Delta M_x}{\Delta M_0} - 1 = \alpha_F \frac{m_x}{m_p} \tag{11}$$

where ΔM_x and ΔM_0 are the torque increment of NBR/CNF composites and NBR, respectively. The m_x and $m_p$are the weight of CNFs and NBR matrix. The values of α_F is positive for all the NBR/CNF composites, this shows the reinforcing effect of CNFs with NBR matrix. From Table 2, the maximum value of α_F was observed at 2 phr CNF reinforced NBR

composites due to the improved reinforcing effect of nanofiber with NBR matrix at this composition. The values of α_F obtained for NBR/CNF composites were found to be greater than α_F values obtained for chitin nanowhiskers reinforced NBR composites (Dominic et al. 2020b).

Mechanical properties of NBR/CNF composites

The tensile properties of CNF reinforced NBR composites are given in Table 3. The prepared NBR/CNF composites show higher tensile strength compared to neat NBR. The NBR/CNF4 composite shows ~ 125 % improvement in tensile strength compared to neat NBR. The stress-strain curves of the prepared NBR/CNF composites are shown in Fig. 3 A. The stress increases linearly with strain initially for all the prepared composites and rubbery deformation happens in the later stage. The improvement in the tensile strength of the prepared nanocomposites can be explained based on the stress transfer theory. At low CNF loading (up to 4 phr), the well-dispersed nanofibers favor effective stress transfer between the matrix and CNFs, and thus helps to prevent the propagation of microcracks. The hydrogen bonding between CNFs and NBR acts as a network, which also helps to transfer the stress continuously from the matrix to the filler. The improvement in the tensile strength of the prepared nanocomposites is in line with the 'Chinese finger trap effect' (Wisittanawat et al. 2014). Thus, the hydrogen bond formation between the hydroxyl groups of nanofibers and the nitrile groups of NBR at the interface, good filler dispersion, and high aspect ratio of the nanofibers led to the improvement in tensile strength of the NBR-CNF composites (Abdul Rashid et al. 2018). The improvement in the tensile strength (~ 125 %) of NBR reinforced with 4 phr of CNFs was observed to be greater than the improvement (~ 116 %) in tensile strength reported by the incorporation of 2 phr chitin nanowhiskers (Dominic et al. 2020b). The deterioration in tensile strength after 4 phr CNF loading was attributed to the agglomeration of nanofibers. At high CNF loading, the nanofibers tend to aggregate and form bundles. Then the fiber-fiber interaction will be more than the fiber-matrix interaction which restricts the effective stress transfer from the matrix to the fiber. The reduced crosslink density and dispersion issue of CNFs are responsible for the low tensile strength of the NBR/CNF6 composite (Cao et al. 2013b)

The elongation at break of NBR, NBR/CNF2, NBR/CNF4, NBR/CNF6 composites was found to be 398 ± 24 %, 321 ± 14 %, 314 ± 28 %, 277 ± 21 % respectively. The nanocomposites show lower elongation at break compared to neat NBR. The modulus at 100 % elongation of NBR, NBR/CNF2, NBR/CNF4, and NBR/CNF6 composites are observed to be 1.07 ± 0.07 MPa, 1.80 ± 0.09 MPa, 1.87 ± 0.04 MPa, and 1.84 ± 0.08 MPa

Table 3 Physico-mechanical and sorption parameters of NBR/CNF nanocomposites

Properties	NBR	NBR/CNF2	NBR/CNF4	NBR/CNF6
Tensile strength (MPa)	2.47 ± 0.15	5.03 ± 0.21	5.55 ± 0.61	4.50 ± 0.49
Elongation at break (%)	398 ± 24	321 ± 14	314 ± 28	277 ± 21
Tear strength (N/mm)	14.54 ± 0.23	28.54 ± 0.56	29.84 ± 0.34	27.08 ± 0.12
Modulus at 100 % elongation (MPa)	1.07±0.07	1.80±0.09	1.87±0.04	1.84±0.08
Hardness (Shore A)	45 ± 1	52 ± 1	53 ± 1	52 ± 1
Compression set (%)	10.20 ± 0.3	16.12 ± 0.23	18.10 ± 0.28	20.10 ± 0.15
Abrasion resistance index (ARI)	195 ± 5	218 ± 2	249 ± 3	215 ± 4
Swelling index (%)	204.24±0.5	196.59±0.7	196.43±0.5	206.21±0.6
Swelling coefficient	1.78±0.02	1.71±0.01	1.70±0.01	1.79±0.02
Crosslink density ($\times 10^{-4}$)	1.51±0.11	1.63±0.13	1.65±0.12	1.34±0.08
n	0.5410	0.5421	0.5785	0.5755
k ($\times 10^{-2}$)	5.722	5.657	4.799	4.562

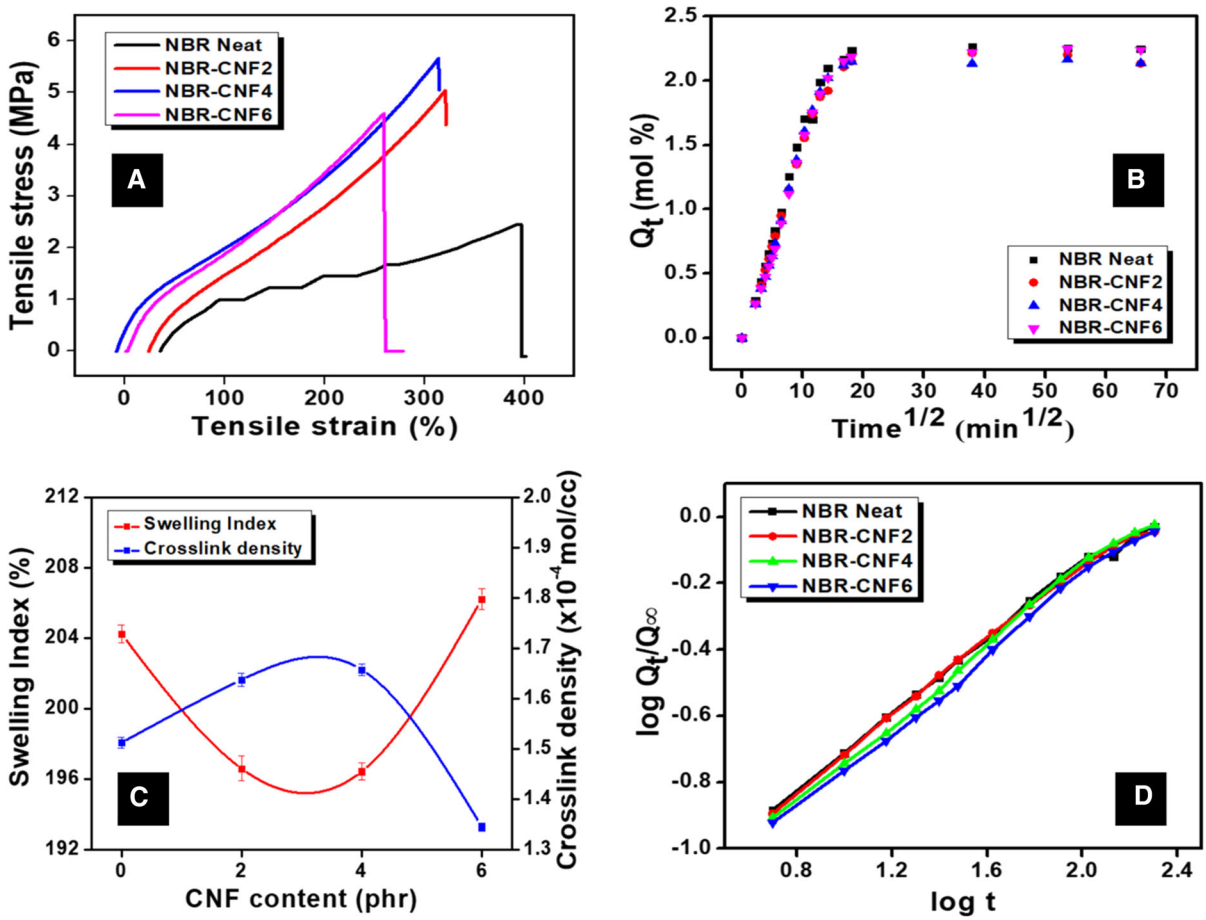

Fig. 3 **a** Stress-strain curves of NBR/CNF composites, **b** Q_t vs. $t^{1/2}$ plot of neat NBR and NBR/CNF composites, (C) Plot showing the swelling index and cross-link density of NBR/CNF. composites, (D) $logQ_t/Q_\infty$ vs. *logt* plot of neat NBRand NBR/CNF composites

respectively. The increase in the modulus of the NBR/CNF nanocomposites is attributed to the improved surface activity and rubber-nanofiber interaction. The confinement of polymer chains by the well-dispersed cellulosic nanofibers provides more stiffness which in turn results in improved modulus values of the prepared NBR/CNF nanocomposites. The modulus drop at high CNF loading was probably due to the agglomeration of nanofibers and lower cross-link density (Cao et al. 2013a). The tear strength of NBR, NBR/CNF2, NBR/CNF4, and NBR/CNF6 are observed to be 14.54 ± 0.23 N/mm, 28.54 ± 0.56 N/mm, 29.84 ± 0.34 N/mm, and 27.08 ± 0.12 N/mm respectively. About 105 % improvement in tear strength was obtained by introducing 4 phr of CNFs in the NBR matrix. The increase in the tear strength is due to the change in the nature of the tear process from a smooth and straight path to a rougher tortuous path. The well-dispersed cellulosic nanofibers can obstruct the tear propagation and more energy is needed to separate the two surfaces which in turn results in higher tear strength. The lower value of the tear strength for sample with 6 phr of CNFs is probably due to the agglomeration of nanofibers. The tensile analysis shows that the dispersion of the cellulose nanofibers in the NBR latex plays a major role in improving the mechanical properties of the prepared composites. By latex stage processing, CNFs can be uniformly dispersed in the NBR matrix which in turn results in effective stress transfer. When the fibers are well dispersed and oriented in the mill direction, they can act as effective stress carriers owing to the superior mechanical properties of the prepared composites (NBR/CNF4). At higher fiber

loading (6 phr), the fiber-fiber agglomeration results in the deterioration of the mechanical properties

The hardness (Shore A) of the prepared nanocomposites is improved considerably compared to neat NBR and the maximum hardness is reported for NBR/CNF4 composite. This suggests that the NBR-CNF4 composite offers more resistance to the reversible deformation by a rigid indenter. The improvement in the hardness of the NBR/CNF4 composite is probably due to the increased stiffness and cross-link density (Sae-Oui et al. 2002). At higher CNF loading, agglomeration of fibers results in lower crosslink density, which may be detrimental to hardness. The abrasion resistance index is highest for NBR/CNF4 composite. About 27 % improvement in the abrasion resistance index is obtained for NBR/CNF4 composite compared to neat NBR. The good dispersion of CNFs, high hardness, and high cross-link density of NBR/CNF4 composite prevents the removal of the matrix by the DIN abrader (Sombatsompop et al. 2004). Among the composites, the abrasion loss is highest for the NBR/CNF6 composite because of the agglomeration of the nanofibers and low cross-link density

It is observed that the compression set values of the prepared nanocomposites increase with an increase in CNF loading. A reverse trend was observed when organoclay, silica, and calcium carbonate were used as fillers in NBR (Sadeghalvaad et al. 2019a). Among the prepared nanocomposites, the compression set is observed to be a minimum for the NBR/CNF2 composite. This suggests that the deformations due to the applied pressure force to NBR/CNF2 composite are greatly reduced by the introduction of well-dispersed CNFs in the polymer matrix. The high compression set value of the NBR/CNF6 composite is attributed to the agglomeration of the nanofibers (Rattanasom et al. 2007)

Swelling studies

The transport of solvent molecules across the NBR matrix depends on the parameters such as the free volume present in the NBR or NBR nanocomposite, interfacial interaction between the nanofibers and NBR, cross-link density, the segmental mobility of the NBR chains, the size of the penetrant molecule, type of the filler/fiber and temperature. The swelling studies provide information on the interfacial adhesion and reinforcing effect of CNFs in NBR. The graphs of solvent uptake (Q_t) with respect to time for NBR and NBR/CNF composites are shown in Fig. 3B. All the prepared samples show a rapid increase in solvent uptake (because of concentration gradient) initially and an equilibrium plateau is reached on the later stage. From Fig. 3B, the sorption of the solvent is lowest at NBR/CNF4 composite. The well-dispersed CNFs can form physical and chemical cross-links with NBR polymer chains which result in decreased chain flexibility that in turn restrict the entry of solvent to the NBR matrix (Moni et al. 2018).

The sorption parameters such as swelling index and swelling coefficient of NBR/CNF composites are given in Table 3. The swelling index of NBR, NBR/CNF2, NBR/CNF4, and NBR/CNF6 composites are observed to be 204.24 ± 0.5, 196.59 ± 0.7, 196.43 ± 0.50, and 206.21 ± 0.60 respectively. The swelling index is minimum for sample reinforced with 4 phr of CNFs. This is due to the decrease in the free volume for this system related to the strong interfacial interaction between CNFs and NBR matrix. At 4 phr CNF loading, the well-dispersed nanofibers can bring the chains closer and keep them intact which in turn results in a low swelling index value of the NBR/CNF4 composite. A similar decrease in swelling index was observed when chitin nanowhiskers were used as a filler in NBR (Dominic et al. 2020). The swelling coefficient of NBR, NBR/CNF2, NBR/CNF4, and NBR/CNF6 composites are found to be 1.78 ± 0.02, 1.71 ± 0.01, 1.70 ± 0.01, and 1.79 ± 0.02 respectively. The tortuous path, tangling effect and the three-dimensional networks created by the cellulosic nanofibers restrict the entry of non-polar solvent molecules into the NBR matrix. Thus, the segmental mobility of the polymer chains and the movement of the solvent molecule between the fiber and polymer interface and polymer-polymer interface get restricted owing to the low value of the swelling coefficient in the prepared NBR/CNF composites except for NBR/CNF6. At high CNF loading (6 phr), CNFs get agglomerated and form bundles. Then the fiber-fiber interaction will be more than the fiber-matrix interaction owing to the high swelling coefficient of NBR/CNF6 composite. The hydrogen bonding between the nitrile rubber and nanofibers may also increase the effective cross-link density, which is also a crucial parameter that influences swelling. The cross-link density is defined as the number of cross-links per unit volume. Higher the cross-link density, lower will be

the degree of swelling (Hoti et al. 2021; Vural et al. 2010). The cross-link density ($\times 10^{-4}$ mol/cc) of NBR, NBR/CNF2, NBR/CNF4, and NBR/CNF6 composites are found to be 1.51 ± 0.11, 1.63 ± 0.13, 1.65 ± 0.12, and 1.34 ± 0.08 respectively. The obtained results of cross-link density of NBR/CNF composites are in line with the swelling index measurements. The cross-link density is maximum for NBR/CNF4 composite. The complex network structure formed by the fiber-fiber and fiber-polymer interactions increased the cross-link density of the material which in turn restricts the entry of solvent molecules to the polymer matrix (Abraham et al. 2013b). It is observed that the cross-link density of the NBR/CNF6 composite is less than that of neat NBR. The decrease in the cross-link density at high CNF loading is attributed to the agglomeration and dispersion issue of cellulosic nanofibers. Boonbumrung et al. reported a similar observation in the cross-link density when MWCNTs are introduced as filler in NBR (Boonbumrung et al. 2016). The swelling analysis shows that the sorption parameters could be considered to predict the physico-mechanical performance of the prepared composites. The reduced segmental mobility of polymer chains is a direct consequence of the effective interaction between the filler and the matrix which in turn results in superior mechanical performance. When the fibers are uniformly distributed in the polymer matrix, the free volume space decreases. The decrease in the free volume space together with the reduced segmental mobility of the polymer chains restrict the entry of solvent to the composite owing to a lower swelling coefficient. Here, the lowest swelling coefficient is reported for NBR/CNF4 composite. The superior tensile properties are also shown by the same composite. A similar trend is also observed when nano $CaCO_3$ is used as filler in NBR (Balachandran and Bhagawan 2012).

The mechanism of transport of toluene across the NBR matrix and CNF reinforced NBR composites can be studied by fitting dynamic swelling data in the Eq. (12) (Southern and Thomas 1967):

$$log Q_t/Q_\infty = \log k + n log t \quad (12)$$

where Q_t and Q_∞ are the mole % uptake of solvent at time t, and at equilibrium, the constant k gives information on the polymer-solvent interactions and structural characteristics of the composites, and the constant n give information on the type of transport.

The value of n and k are determined from the slope and intercept of the graph of log Qt/Q ∞ versus log$t$. The value of n = 0.5 shows a Fickian transport, where the penetration of liquid molecules is slower than the rate of polymer chain relaxation (Jose et al. 2017). If the value n = 1 the transport is non-Fickian, where the penetration of liquid molecules is faster than the rate of polymer chain relaxation. If the value of n lies between 0.5 and 1 then the transport is anomalous. Sometimes a 'Less Fickian' mode of transport is also possible when the liquid penetration becomes much lower than polymer chain relaxation, i.e., n<0.5. For all the prepared composites, the n values are between 0.5 and 1 suggests a deviation from the normal Fickian transport and can be considered as anomalous. Visakh et al. reported similar values for n when natural rubber is reinforced with cellulosic nanofibers (Visakh et al. 2012a). The anomalous mode of transport arises because of the coupling of Fickian and non-Fickian behavior. The n value is associated with the response time of NBR segments to the swelling stress and the rearrangement of the polymer chains to provide room for the penetration of the solvent molecules. The segmental motion of NBR chains gets restricted by reinforcing the NBR matrix with CNFs. The slow relaxation of the polymer chains in the presence of CNFs leads to an anomalous transport behavior and a marginal increase in the value of n (Abraham et al. 2015). The magnitude of k signifies the polymer-solvent interaction and structural characteristics of the composite. The value of k is found to be less for NBR/CNF composites compared to neat NBR. This also supports the fact that CNFs can effectively restrict the interaction between the polymer and the solvent molecules. Abraham et al. reported a similar trend in k values when styrene-butadiene rubber is reinforced with MWCNTs (Abraham et al. 2015).

Fractographic studies of NBR/CNF composites

The failure of CNF reinforced NBR composites mainly occur by the breakage of cellulose nanofibers, and the pull-out of fibers from the NBR matrix. Figure 4(A), 4(B), and 4(C) represent the SEM images of the fractured surfaces of NBR/CNF2, NBR/CNF4, and NBR/CNF6 composites under 600x magnification. Figure 4(D), 4(E), and 4(F) represent the SEM images of the fractured surfaces of NBR/CNF2, NBR/

CNF4, NBR/CNF6 composites under 3000x magnification. The smooth continuous phase is seen in the NBR/CNF2 composite [Fig. 4(A) and 4(D)], is an evidence of better interfacial compatibility between the fiber and matrix. No direct separation between CNFs and the NBR matrix was observed at lower filler loading. At low filler loading (2, 4 phr), the cellulosic nanofibers were neither debonded nor pulled-off from the matrix owing to the better interfacial adhesion between CNFs and NBR. A similar fractographic structural pattern was observed in the case of NBR/CNC composites (Suryani et al. 2017). As the fiber content increases, the surface became rough and with irregular fracture patterns. This shows the change in the fracture mechanism. The roughness and special structure pattern [Fig. 4(B) and 4(E)] of the tensile fractured surface of the NBR/CNF4 composite shows better fiber-matrix interaction and effective stress transfer. Figure 4(C) shows agglomerates of CNFs, indicate the inhomogeneous distribution of CNFs in NBR at higher loading (6 phr). The magnified image (Fig. 4(F)) of the tensile fractured surface of the NBR/CNF6 composite showed dispersion issue, deformations, tiny protrusions of CNFs, and clear phase separation. The aggregates of CNFs act as nucleating sites for crack propagation, which will ultimately result in inferior mechanical properties (Correia et al. 2017). No such aggregates are visible in the fractographic images of NBR/CNF2 and NBR/CNF4 composites. The fractographic studies of the prepared nanocomposites are in line with the tensile and sorption results of the NBR-CNF composites. The schematic of the possible hydrogen bonding between CNFs and NBR is shown in Fig. 5.This illustration is drawn based on FTIR, XRD and microscopic observations on the interfacial adhesion between CNFs and NBR.

Thermogravimetric and DSC analysis of NBR/CNF composites

The thermal analysis data of NBR and CNF reinforced NBR composites are given in Table 4. The TG and DTG curves of the composites are shown in Fig. 6 A

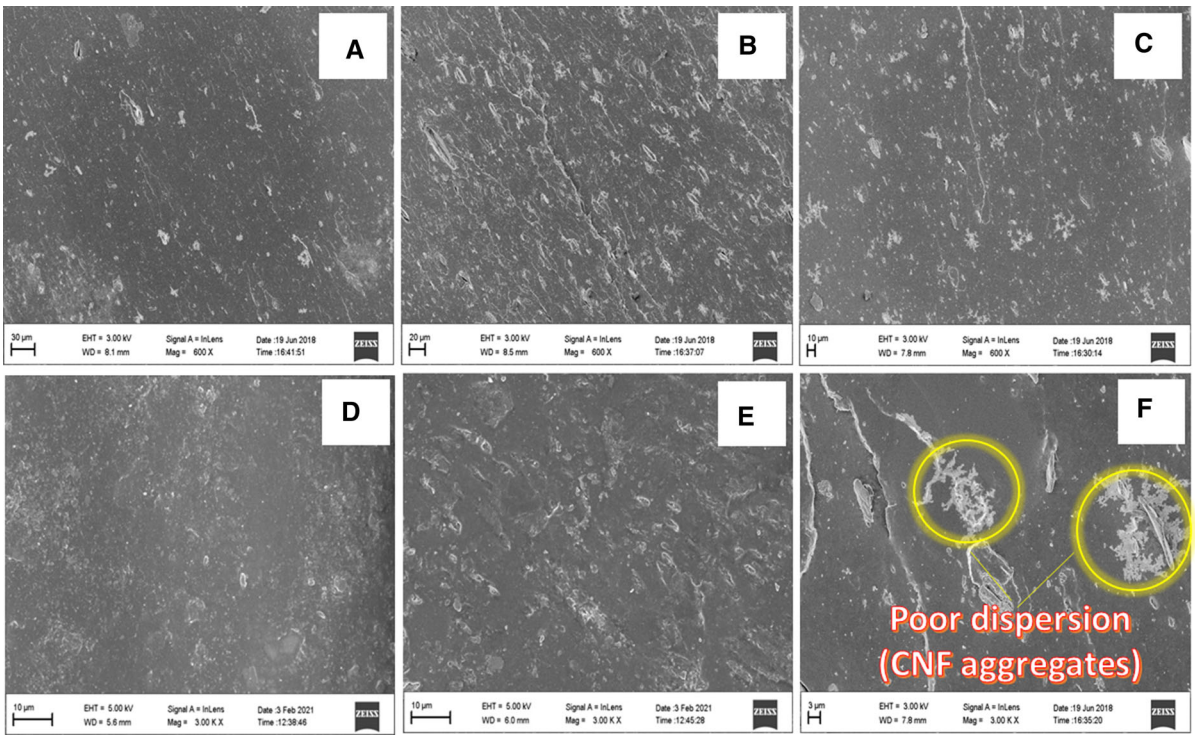

Fig. 4 SEM images of tensile fractured samples of NBR/CNF2 (**a**) & (D), NBR/CNF4 (**b**) & (**e**), NBR/CNF6 (**c**) & (**f**) composite under two different magnifications 600× and 3000×)

& 6B. The initial weight loss at ~ 100 °C is due to the loss of moisture present in the samples. The degradation of the NBR occurs between 350 and 500 °C in all the prepared composites. The reason for the thermal degradation is polymer chain scission and NBR/CNF cross-link breakage. The onset decomposition temperature (T_{on}) of NBR, NBR/CNF2, NBR/CNF4, and NBR/CNF6 composites are observed to be 375 °C, 401 °C, 393 °C, and 402 °C respectively. About 26 °C increase in T_{on} was observed when 2 phr CNFs were introduced into the NBR matrix. Abdul Rashid et al. reported a 5 °C rise in T_{on} when 2 phr cellulose nanocrystals (CNCs) was used as filler in NBR (Abdul Rashid et al. 2018). The well-dispersed CNFs act as a heat barrier and channelize the heat dissipation in the matrix which in turn prevents the NBR chain scission. The immobilization of the macromolecular chains by the cellulosic nanofibers was probably responsible for the improved onset degradation temperature of the prepared nanocomposites. The temperature at which 50 % decomposition occurs (T_{50}) for NBR recorded an increase from 450 to 461 °C by the introduction of 2 phr of CNFs. The interfacial interaction between the filler and polymer reduces the segmental mobility of the polymer phase in the proximity of CNFs when heating is introduced. Besides, the hydrogen bonding between CNFs and NBR increases the cross-link-density and rigidity of the system which in turn results in higher thermal stability (Abdul Rashid et al. 2018). The interfacial interaction between the CNFs and the NBR matrix protects the fiber by keep away from the direct exposure with the temperature which in turn results in higher thermal stability (Asim et al. 2020).

From the derivative thermogram curve (DTG), the temperature at which maximum degradation occurs (T_{max}) of prepared composites were recorded. The T_{max} of NBR, NBR/CNF2, NBR/CNF4, and NBR/CNF6 composites are found to be 449 °C, 454 °C, 461 °C, and 459 °C, respectively. About 12 °C rise in T_{max} is observed when 4 phr of CNFs is introduced as filler in NBR. Abdul Rashid et al. reported that the T_{max} of NBR can be improved from 451 to 465 °C by the introduction of 2 phr CNCs (Abdul Rashid et al. 2018). The increase in T_{max} of the prepared composites is mainly due to the restricted thermal motion of NBR chains that are bound to the surface of CNFs (Sreenath et al. 2017). The residue of the prepared nanocomposites at 500 °C was found to be higher at higher CNF loading. The high residue shows the presence of crystalline cellulose in CNFs, which is intrinsically flame resistant. The increase in the residue content reflects the successful incorporation of CNFs in the NBR matrix and better thermal stability.

The kinetic parameters of the thermal decomposition of CNF reinforced NBR nanocomposites are evaluated using the Coats and Redfern method (Coats and Redfern 1964).

The activation energy can be calculated using the Eq. (13):

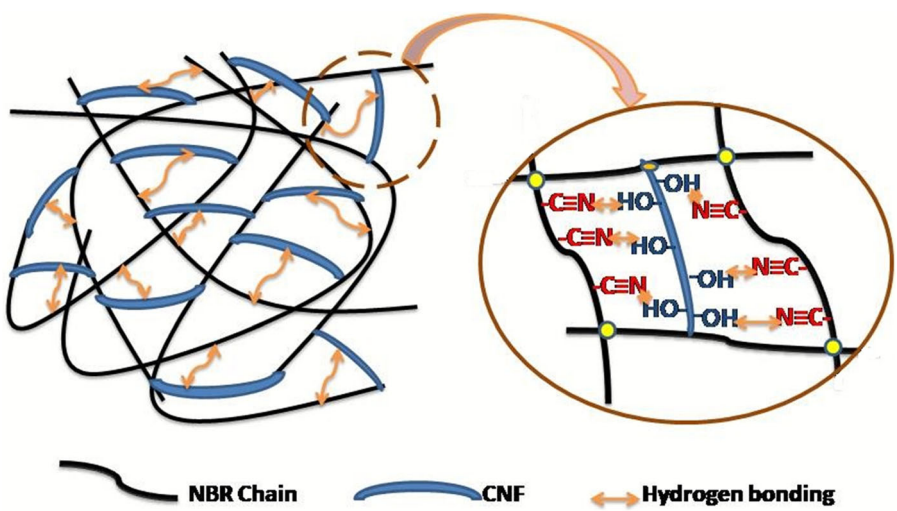

Fig. 5 A possible molecular-level view of the hydrogen bonding between the NBR and CNFs

Table 4 Thermogram data of NBR/CNF composites

Samples	T_{on} (°C)	T_{50} (°C)	T_{max} (°C)	Residue at 500 °C (%)	Activation energy, E_a (kJ/mol)	R^2
NBR	375	450	449	19.46	183.64	0.9942
NBR/CNF2	401	461	454	21.93	164.91	0.9991
NBR/CNF4	393	459	461	22.39	161.58	0.9896
NBR/CNF6	402	461	459	23.14	175.44	0.9978

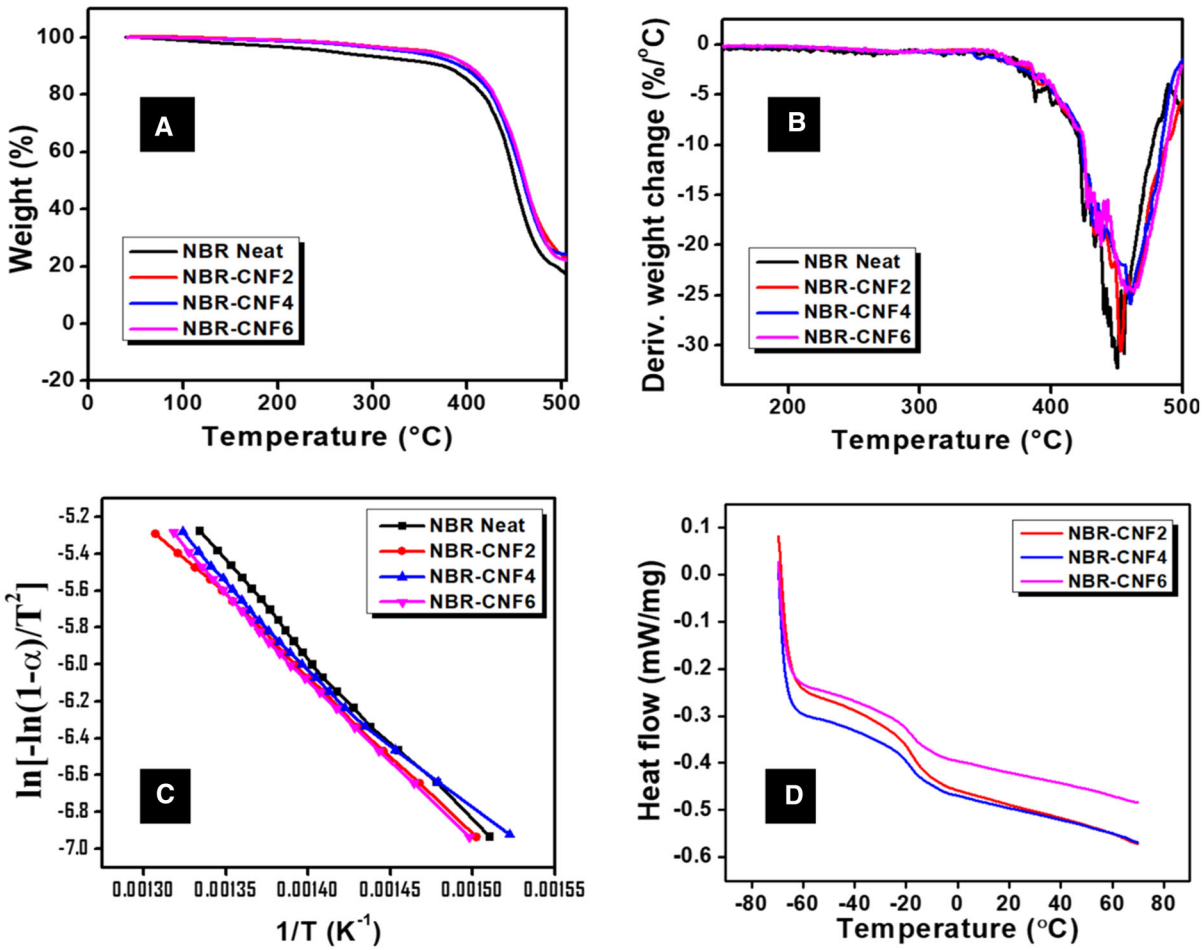

Fig. 6 (**a**) & (**b**) TG and DTG curves of NBR/CNF composites (**c**) kinetics of thermal decomposition of NBR/CNF composites using Coats-Redfern equation (**d**) DSC curves of NBR/CNF composites.

$$\ln\left(\frac{-\ln(1-\alpha)}{T^2}\right) = \ln\left(\frac{AR}{\beta E_a}\right) - \frac{E_a}{RT} \quad (13)$$

where, T is the heating temperature, A is the Arrhenius- factor, E_a is the activation energy, R is the gas constant, and β the heating rate. The parameter α is represented as Eq. (14):

$$\alpha = \frac{C_0 - C}{C_0 - C_f} \quad (14)$$

.

Here C_0, C and C_f are the mass of the material at the initial temperature, temperature chosen and final temperature, respectively. The plot of $\ln\left(\frac{-\ln(1-\alpha)}{T^2}\right)$ vs. $1/T$ for neat NBR and NBR/CNF composites is given

in Fig. 6 C. The regression analysis gives the slope, intercept, and concurrency value (R^2) of the thermal degradation process of NBR/CNF composites. The value of E_a can be calculated from the slope of the curve. The activation energies of NBR, NBR/CNF2, NBR/CNF4, and NBR/CNF6 are found to be 183.64 kJ/mol, 164.91 kJ/mol, 161.58 kJ/mol, and 175.44 kJ/mol respectively. Lower E_a values are observed for NBR-CNF composites when compared to neat NBR. The kinetic study of the thermal decomposition of the prepared nanocomposites showed that the incorporation of CNFs in the NBR matrix accelerates thermal degradation. This is somewhat paradoxical to the result obtained for T_{on}, T_{50}, and T_{max} values of NBR/CNF composites. These results are in agreement with Abdul Rashid et al. (Abdul Rashid et al. 2018). They have reported that E_a of pristine NBR decreased from 88.13 kJ/mol to 56.17 kJ/mol with the introduction of 2 phr CNCs, whereas T_{max} was improved from 451 to 465 °C. The possible explanation of the above observation is as follows. The char formed by the decomposition of CNFs may act as a protective barrier to both mass and energy transfer which in turn results in delaying thermal degradation of the NBR-CNF composites. Once the applied heat exceeds a threshold value, the barrier effect of CNFs became ineffective and the plenty of oxygen present in the backbone of CNFs facilitates the thermal degradation of NBR, which leads to a decrease in the activation energy. Li et al. reported a similar observation when porous rice bran carbon was used as a filler in NBR (Li et al. 2014).

The DSC profile of NBR/CNF composites are shown in Fig. 6D. The glass transition temperature (T_g) of the prepared NBR/CNF composites depends upon its structure and segmental mobility of polymer chains. The T_g values of NBR/CNF2, NBR/CNF4, NBR/CNF6 composites are found to be −21.9 °C, −21.7 °C, −22.3 °C respectively. The DSC analysis shows that no significant change in T_g is observed among the prepared composites.

Dynamic mechanical analysis

To study the viscoelastic properties and constrained region, the dynamic mechanical analysis (DMA) was conducted for the prepared composites. The DMA data are summarized in Table 5. The dynamic mechanical properties of the prepared composites were mainly influenced by the nature of the matrix, type of the filler, the concentration of the filler, and the interface. Figure 7 shows the change in storage modulus (E′) (Fig. 7A), loss modulus (E″) (Fig. 7B), and loss tangent (tanδ) (Fig. 7 C) of the prepared NBR/CNF composites as a function of temperature. The E′ is a parameter to determine the maximum energy stored in the prepared nanocomposites during one cycle of oscillation (Formela et al. 2016). It is a measure of the stiffness and elastic properties of the prepared nanocomposites. The E' of NBR, NBR/CNF2, NBR/CNF4, and NBR/CNF6 composites at −40 °C (glassy region) is found to be 1189 MPa, 1041 MPa, 1970 MPa and 1833 MPa respectively. The analysis showed that the glassy E′ of NBR/CNF4, NBR/CNF6 composites is found to be greater than that of neat NBR. Surprisingly, in the glassy region, the storage modulus of the NBR/CNF2 composite was found to be less than that of pristine NBR. Liu et al. reported similar observations in the glassy E′ when 1 % chitin nanocrystals were used as a filler in natural rubber (NR) (Liu et al. 2018). They inferred that the slight decrease in the glassy E′ of NR-chitin

Table 5 DMA data of NBR/CNF composites (NBR, previously published values (Dominic et al. 2020b))

Properties	NBR	NBR/CNF2	NBR/CNF4	NBR/CNF6
T_g (w.r.to tan δ max) (°C)	−4.09	2.10	2.67	2.13
T_g (w.r.to E'' max) (°C)	−11.15	−9.51	−9.76	−10.05
Storage modulus at -40 °C (MPa)	1189	1041	1970	1833
Storage modulus at 25 °C (MPa)	3.651	6.043	8.267	7.1847
Maximum Tan δ	1.535	0.998	1.071	1.100
$\beta\varnothing$	–	0.538	0.433	0.395
C_v	0	0.0845	0.0693	0.0636
A	–	−0.3360	−0.2732	−0.2376

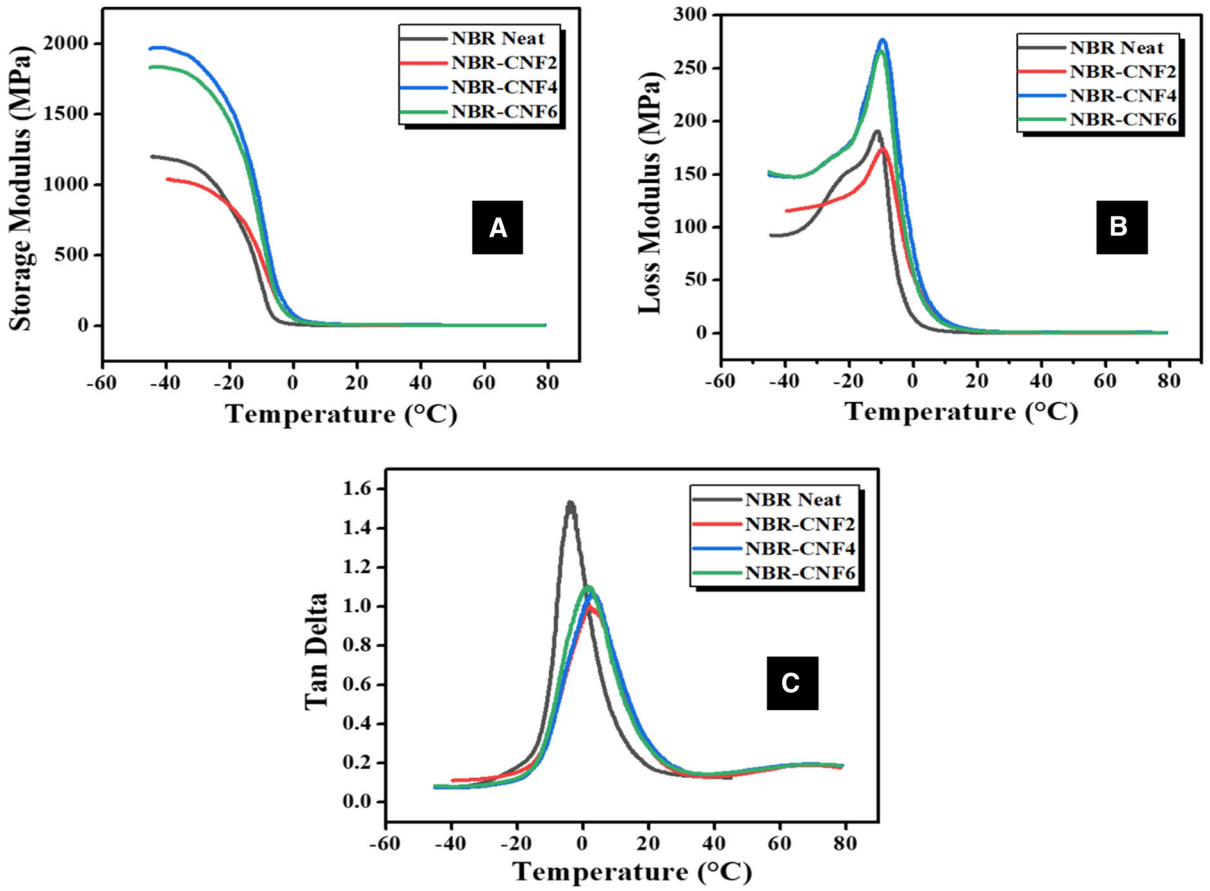

Fig. 7 **a** Plot of storage modulus versus temperature, **b** Plot of loss modulus versus temperature, and **c** Plot of loss tangent (tan δ) versus temperature

nanocrystal composite at lower loadings of nanofiller (1 %) was probably due to the change in the conformation and free volume of the rubber. The immobilization of NBR molecular chains by CNFs was probably the reason for the higher E' of NBR/CNF4 and NBR/CNF6 composites. A sharp transition from glassy to the rubbery state was observed at around −20 °C for all the prepared composites because of the glass transition process. At temperature higher than T_g, the E′ drops and later a plateau is achieved. The rubbery modulus at 25 °C for NBR, NBR/CNF2, NBR/CNF4, and NBR/CNF6 composites is observed to be 3.65 MPa, 6.04 MPa, 8.26 MPa, and 7.18 MPa respectively. Around 126 % increase in rubbery modulus is observed for NBR/CNF4 composite compared to neat NBR. Mariano et al. reported that the rubbery modulus is greatly influenced by the crystallinity index of the nanofiller (Mariano et al. 2016). In other words, the presence of crystalline domains of CNFs substantially improve the rubbery modulus of NBR. Dominic et al. also reported an improvement (68 %) in the rubbery modulus of NBR, when chitin nanowhiskers (2 phr) were used as reinforcing filler (Dominic et al. 2020).

Loss modulus (E'') is the energy lost by the NBR/CNF composites during the DMA analysis. The increase in the peak height ofE'' of the nanocomposites is due to the heat dissipation caused by the filler-filler interaction, filler-polymer interaction during DMA test (Prasertsri and Rattanasom 2012). The T_g was determined from the maximum of E" versus temperature curve. The T_g of NBR, NBR/CNF2, NBR/CNF4, and NBR/CNF6 was recorded as −11.15 °C, −9.51°C, −9.76 °C, and −10.05°C respectively. The positive shift in the T_g of the nanocomposites showed the reinforcing effect of CNFs. The hydrogen bonding

between NBR and CNFs at the interface restricts the free movement of the rubber macromolecular chains resulting in an increase in the T_g values of the nanocomposites (Cao et al. 2013b).

Loss tangent (tan δ) is the ratio of E" and E′. The value of tan δ depends on the mobility of the polymer chains (Chen et al. 2015). The tan δ peak height of NBR, NBR/CNF2, NBR/CNF4, and NBR/CNF6 are observed to be 1.535, 0.998, 1.071, and 1.100 respectively. The higher tan δ peak corresponds to a high chain mobility (Zhao et al. 2019). The decrease in tan δ peak height of NBR/CNF composites compared to pristine NBR is probably due to the hindering of the movement of rubber molecular chains by the well-dispersed CNFs (Joseph et al. 2010).The high degree of dispersion of nanofiber results in mechanical interlocking with the NBR matrix which in turn results in intertwining of macromolecular rubber chains. The good dispersion and interaction of CNFs with the NBR matrix decrease the "active" bulk rubber during the dynamic transition process resulting in the reduction in tan δ peak height (Sreenath et al. 2020). The tan δ values showed that the cellulosic nanofibers play a crucial role in decreasing the damping of the prepared nanocomposites. Ziegel & Romanov related the maximum tan δ of the filled and unfilled system in accordance with the Eq. (15) (Ziegel and Romanov 1973)

$$\tan \delta_{mf} = \tan \delta_{mu}/1 + \beta\varnothing \quad (15)$$

Where, $\tan\delta_{mf}$ and $\tan\delta_{mu}$ represent the maximum tan δ value of the NBR composites and neat NBR respectively, $\beta$is the interaction parameter determining the interfacial interaction between the nanofiber and NBR matrix, $\phi$is the volume fraction of nanofiber. The $\beta\phi$values of NBR/CNF2, NBR/CNF4, NBR/CNF6 composites were found to be 0.538, 0.433, and 0.395 respectively. The combination parameter '$\beta\phi$' value reported in this study is superior to the $\beta\phi$ value reported for the NBR-precipitated silica system (Boonbumrung et al. 2016). The high value of $\beta\phi$ at 2 and 4 phr CNF loading showed higher reinforcing efficiency and better interfacial compatibility of CNFs in the NBR matrix.

The T_g with respect to maximum tan δ of pure NBR, NBR/CNF2, NBR/CNF4, and NBR/CNF6 composites is recorded as −4.09 °C, 2.10 °C, 2.67 °C, and 2.13 °C respectively. The T_g of NBR increased by about 6 °C with the introduction of 2 phr CNF. The positive shift in the T_g of the prepared NBR-CNF composites showed the increased cross-link density and matrix-filler interaction (Dileep et al. 2020). Ambilkar et al. reported a similar positive shift in the T_g in the case of NBR- zirconia composites (Ambilkar et al. 2020). To study more about the volume fraction of the polymer chains immobilized, the constrained region (C_v) and adhesion parameter (A) of the CNF reinforced NBR composites were evaluated. The C_v values of NBR/CNF2, NBR/CNF4, and NBR/CNF6 composites are observed to be 0.0845, 0.0693, and 0.0636 respectively. The high C_v values of the composites (2 and 4 phr) is owing to their better cross-link density and good interfacial interaction. The CNFs can effectively restrict the segmental motion of the polymer chain because of hydrogen bonding interaction and nano-size effect. At higher CNF loading, the fibers became aggregated and the filler-filler interactions over ways filler-polymer interactions. That might be responsible for the low C_v value of NBR-CNF6 composite. The adhesion factor 'A' was found to be the lowest for the NBR-CNF2 composite followed by 4 phr composite. The lower the value of A, the higher will be the interfacial adhesion between CNFs and the NBR matrix (Dominic et al. 2020).

Conclusions

The manufacturing of value-added products from agricultural waste materials is an emerging area of green engineering. Here, we demonstrated that the cellulose nanofibers extracted from the parasitic plant *Cuscuta reflexa* could be used as potent green filler in NBR for high-performance elastomeric applications. The FTIR and XRD analysis of NBR/CNF composites ascertained the interfacial interaction between CNF and NBR. The cure time and scorch time of NBR/CNF composites were shown to be greater than that of neat NBR. The cure rate index was reduced in the presence of CNFs. The tensile and tear strength of NBR matrix presented an increase of ∼ 125 % and ∼ 105 % respectively at 4 phr CNF loading. The remarkable improvement in the modulus, hardness, and abrasion resistance index of NBR-CNF4 composite presents the reinforcing action of CNFs. The compression set of the prepared composites increase with an increase in CNF

content. The swelling rate in toluene was minimum for NBR/CNF4 composite owing to their higher crosslink density. The mechanism of transport of the solvent molecules was found to be anomalous rather than Fickian. The T_{on}, T_{50}, and T_{max} significantly improved by the addition of CNFs in the NBR matrix. The T_{on}, $T_{50,}$ and T_{max} of NBR showed an increase of 26 °C, 11 °C and 15 °C respectively at 2 phr CNF loading. The kinetic parameters of the thermal degradation of the prepared NBR/CNF nanocomposites were evaluated from the thermogravimetric curves using Coats-Redfern method. Lower activation energy (E_a) values were observed for NBR/CNF composites when compared to neat NBR. The fractographic studies showed effective stress transfer in the NBR/CNF composites at low CNF loading. Agglomeration of CNFs was observed at 6 phr CNF loading which might be the reason for their inferior physico-mechanical properties. From the DSC analysis, the T_g values of NBR/CNF2, NBR/CNF4, NBR/CNF6 composites were found to be −21.9 °C, −21.7 °C, −22.3 °C respectively. The DMA analysis shows that the T_g of neat NBR can be increased by 6 °C by incorporating 4 phr CNFs ascribed to the reinforcing action of CNFs. The decrease in the loss tangent peak height in the NBR/CNF composites proved the confinement of NBR chains by well-dispersed CNFs. Based on the presented results, it can be concluded that the CNFs can be used as sustainable green filler in NBR for elastomeric applications.

Credit authorship contribution statement.

MD C.D.: Conceptualization, Methodology, Visualization, Writing- Original draft. RJ: Supervision. P.M. SB: Supervision. AS.: Investigation. J. P.A.: Data curation. TJ: Data curation. DP: Resources, KF: Writing, Reviewing and Editing, SS: Writing, Reviewing and Editing, JP: Writing, Reviewing and Editing, MRS: Methodology, Writing, Reviewing and Editing.

Acknowledgments The authors greatly acknowledge SAIF STIC, CUSAT for chemical analysis and J J Murphy Research Centre, Kerala for rubber compounding.

Availability of data and material My research didn't generate any data or I reused existing data.

Declarations

Conflict of interest The authors declare no conflicts of interest.

Human and animal participants This article does not contain any studies involving animals or human participants performed by any of the authors.

References

Abdul Rashid ES, Muhd Julkapli NB, Abdul Hadi Yehya W (2018) Reinforcement effect of nanocellulose on thermal stability of nitrile butadiene rubber (NBR) composites. JAppl Polym Sci 135:46594. https://doi.org/10.1002/app.46594

Abraham E, Deepa B, Pothan LA et al (2013a) Physicomechanical properties of nanocomposites based on cellulose nanofibre and natural rubber latex. Cellulose 20:417–427. https://doi.org/10.1007/s10570-012-9830-1

Abraham J, Maria HJ, George SC et al (2015) Transport characteristics of organic solvents through carbon nanotube filled styrene butadiene rubber nanocomposites: the influence of rubber – filler interaction, the degree of reinforcement and morphology. Phys Chem Chem Phys 17:11217–11228. https://doi.org/10.1039/C5CP00719D

Abraham E, Thomas MS, John C et al (2013b) Green nanocomposites of natural rubber/nanocellulose: Membrane transport, rheological and thermal degradation characterisations. Ind Crops Prod 51:415–424. https://doi.org/10.1016/j.indcrop.2013.09.022

Ambilkar SC, Bansod ND, Kapgate BP et al (2020) In Situ Zirconia: A Superior Reinforcing Filler for High-Performance Nitrile Rubber Composites. ACS Omega 5:7751–7761. https://doi.org/10.1021/acsomega.9b03495

Asim M, Paridah MT, Chandrasekar M et al (2020) Thermal stability of natural fibers and their polymer composites. Iran Polym J 29:625–648. https://doi.org/10.1007/s13726-020-00824-6

Azman Mohammad Taib MN, Yeheye W, Muhd Julkapli N (2020) Synthesis and characterization of nanocrystalline cellulose as reinforcement in nitrile butadiene rubber composites. Cellul Chem Technol 54:11–25

Bahloul A, Kassab Z, Bouchti M, El et al (2021) Micro- and nano-structures of cellulose from eggplant plant (Solanum melongena L) agricultural residue. Carbohydr Polym 253:117311. https://doi.org/10.1016/j.carbpol.2020.117311

Balachandran M, Bhagawan SS (2012) Mechanical, thermal and transport properties of nitrile rubber (NBR)-Nanoclay composites. J Polym Res 19:1–10. https://doi.org/10.1007/s10965-011-9809-x

Boonbumrung A, Sae-oui P, Sirisinha C (2016) Reinforcement of multiwalled Carbon Nanotube in Nitrile Rubber. In Comparison with Carbon Black, Conductive Carbon Black, and Precipitated Silica. J Nanomater 2016:1–8. https://doi.org/10.1155/2016/6391572

Bryan E, Welding GN (1964) Estimation, from Swelling, of the Structural Contribution of Chemical Reactions to the

Vulcanization of Natural Rubber. Part II. Estimation of Equilibrium Degree of Swelling. Rubber Chem Technol 37:571–575. https://doi.org/10.5254/1.3540349

Cao X, Xu C, Wang Y et al (2013a) New nanocomposite materials reinforced with cellulose nanocrystals in nitrile rubber. Polym Test 32:819–826. https://doi.org/10.1016/j.polymertesting.2013.04.005

Cao X, Xu C, Wang Y et al (2013b) New nanocomposite materials reinforced with cellulose nanocrystals in nitrile rubber. Polym Test 32:819–826. https://doi.org/10.1016/j.polymertesting.2013.04.005

Chakrabarty A, Teramoto Y (2018) Recent Advances in Nanocellulose Composites with Polymers: A Guide for Choosing Partners and How to Incorporate Them. Polymers 10:517. https://doi.org/10.3390/polym10050517

Chen WJ, Gu J, Xu SH (2014) Exploring nanocrystalline cellulose as a green alternative of carbon black in natural rubber / butadiene rubber / styrene-butadiene rubber blends. eXPRESS Polym Lett 8:659–668. https://doi.org/10.3144/expresspolymlett.2014.69

Chen Y, Zhang Y, Xu C, Cao X (2015) Cellulose nanocrystals reinforced foamed nitrile rubber nanocomposites. Carbohydr Polym 130:149–154. https://doi.org/10.1016/j.carbpol.2015.05.017

Coats AW, Redfern JP (1964) Kinetic Parameters from Thermogravimetric Data. Nature 201:68–69. https://doi.org/10.1038/201068a0

Correia CA, Oliveira LM de, Valera TS et al (2017) The Influence of Bleached Jute Fiber Filler on the Properties of Vulcanized Natural Rubber. Mater Res 20:466–471. https://doi.org/10.1590/1980-5373-mr-2017-0126

Dileep P, Varghese GA, Sivakumar S, Narayanankutty SK (2020) An innovative approach to utilize waste silica fume from zirconia industry to prepare high performance natural rubber composites for multi-functional applications. Polym Test 81:106172. doi:https://doi.org/10.1016/j.polymertesting.2019.106172

Dominic CDM, Joseph R, Begum PMS, et al (2020a) Cellulose Nanofibers Isolated from the Cuscuta Reflexa Plant as a Green Reinforcement of Natural Rubber. Polymers 12:814. https://doi.org/10.3390/polym12040814

Dominic CDM, Joseph R, Begum PMS et al (2020b) Chitin nanowhiskers from shrimp shell waste as green fi ller in acrylonitrile- butadiene rubber: Processing and performance properties. Carbohydr Polym 245:116505. https://doi.org/10.1016/j.carbpol.2020.116505

El-sabbagh SH, Mohamed OA (2011) Recycling of Chrome-Tanned Leather Waste in Acrylonitrile Butadiene Rubber. J Appl Polym Sci 121:979–988. https://doi.org/10.1002/app

Flauzino Neto WP, Mariano M, da Silva ISV et al (2016) Mechanical properties of natural rubber nanocomposites reinforced with high aspect ratio cellulose nanocrystals isolated from soy hulls. Carbohydr Polym 153:143–152. https://doi.org/10.1016/j.carbpol.2016.07.073

Flory PJ, Rehner J (1943) Statistical mechanics of cross-linked polymer networks I. Rubberlike elasticity. J Chem Phys. 11:512. https://doi.org/10.1063/1.1723791

Formela K, Hejna A, Piszczyk Ł et al (2016) Processing and structure–property relationships of natural rubber/wheat bran biocomposites. Cellulose 23:3157–3175. https://doi.org/10.1007/s10570-016-1020-0

Foster EJ, Moon RJ, Agarwal UP et al (2018) Current characterization methods for cellulose nanomaterials. ChemSoc Rev 47:2609–2679. https://doi.org/10.1039/c6cs00895j

Hubbe MA, Rojas OJ, Lucia LA et al (2008) Cellulosic nanocomposites: a review. BioResources 3:929–980

Ismail H, Ahmad HS (2013) The Properties of Acrylonitrile-Butadiene Rubber (NBR) Composite with Halloysite Nanotubes (HNTs) and Silica or Carbon Black. Polym Plast Technol Eng 52:1175–1182. https://doi.org/10.1080/03602559.2013.769577

Jiang W, Gu J (2020) Nanocrystalline cellulose isolated from different renewable sources to fabricate natural rubber composites with outstanding mechanical properties. Cellulose 27:5801–5813. https://doi.org/10.1007/s10570-020-03209-3

Jose T, Moni G, Salini S et al (2017) Multifunctional multi-walled carbon nanotube reinforced natural rubber nanocomposites. Ind Crop Prod 105:63–73. https://doi.org/10.1016/j.indcrop.2017.04.047

Joseph S, Appukuttan SP, Kenny JM et al (2010) Dynamic mechanical properties of oil palm microfibril-reinforced natural rubber composites. J Appl Polym Sci 117:1298–1308. https://doi.org/10.1002/app.30960

Khattab MM, Abdel-Hady NA, Dahman Y (2017) Cellulose nanocomposites: Opportunities, challenges, and applications. In: Cellulose-Reinforced Nanofibre Composites. Woodhead Publishing, pp 483–516

Kruželák J, Hudec I, Dosoudil R, Sýkora R (2015) Investigation of strontium ferrite activity in different rubber matrices. J Elastomers Plast 47:277–290. https://doi.org/10.1177/0095244313507809

Kulshrestha U, Gupta T, Kumawat P et al (2020) Cellulose nanofibre enabled natural rubber composites: Microstructure, curing behaviour and dynamic mechanical properties. Polym Test 106676. https://doi.org/10.1016/j.polymertesting.2020.106676

Li M-C, Zhang Y, Cho UR (2014) Mechanical, Thermal and Friction Properties of Rice Bran Carbon / Nitrile Rubber Composites : Influence of Particle Size and Loading. Mater Des 63:565–574. https://doi.org/10.1016/j.matdes.2014.06.032

Lin N, Dufresne A (2014) Nanocellulose in biomedicine: Current status and future prospect. Eur Polym J 59:302–325. https://doi.org/10.1016/j.eurpolymj.2014.07.025

Liu Y, Liu M, Yang S et al (2018) Liquid Crystalline Behaviors of Chitin Nanocrystals and Their Reinforcing Effect on Natural Rubber. ACS Sustainble Chem Eng 6:325–336. https://doi.org/10.1021/acssuschemeng.7b02586

Mariano M, El N, Dufresne A (2016) Cellulose nanocrystal reinforced oxidized natural rubber nanocomposites. Carbohydr Polym 137:174–183. https://doi.org/10.1016/j.carbpol.2015.10.027

Mariano M, Kissi N, El, Dufresne A (2014) Cellulose Nanocrystals and Related Nanocomposites: Review of some Properties and Challenges. J Polym Sci Part B: Polym Phys 52:791–806. https://doi.org/10.1002/polb.23490

Mohamad Taib MNA, Muhd Julkapli N, Yehye WA, Abdul Hamid SBOA (2017) Microstructures of Nanocellulose and Reinforcement in Nitrile Butadiene Rubber (NBR)

Composites. Solid State Phenom 264 SSP:124–127. https://doi.org/10.4028/www.scientific.net/SSP.264.124
Moni G, Abraham J, Kurian C, Joseph A, George SC (2018) Effect of reduced graphene oxide on the solvent transport characteristics and sorption kinetics of fluoroelastomer nanocomposites. Phys Chem Chem Phys 20:17909–17916. https://doi.org/10.1039/C8CP02411A
Nunes RCR (2017) Rubber nanocomposites with nanocellulose. In: Progress in Rubber Nanocomposites. Woodhead Publishing, pp 463–494
Paul C, Debnath B, Paul C (2019) Plant Science Today species. Plant Science Today 6:147–150
Prasertsri S, Rattanasom N (2012) Fumed and precipitated silica reinforced natural rubber composites prepared from latex system: Mechanical and dynamic properties. Polym Test 31:593–605. https://doi.org/10.1016/j.polymertesting.2012.03.003
Rajkumar K, Ranjan P, Thavamani P, Jeyanthi P (2013) Dispersion studies of nanosilica in NBR based polymer nanocomposite. Rasayan J Chem 6:122–133
Ramesan A, Nihmath M (2017) Fabrication, Characterization and Dielectric Studies of NBR / Hydroxyapatite Nanocomposites. J Inorg Organomet Polym Mater 27:481–489. https://doi.org/10.1007/s10904-016-0490-8
Rattanasom N, Saowapark T, Deeprasertkul C (2007) Reinforcement of natural rubber with silica / carbon black hybrid filler. Polym Test 26:369–377. https://doi.org/10.1016/j.polymertesting.2006.12.003
Rosli NA, Ahmad I, Anuar FH, Abdullah I (2019) Effectiveness of cellulosic Agave angustifolia fibres on the performance of compatibilised poly(lactic acid)-natural rubber blends. Cellulose 26:3205–3218. https://doi.org/10.1007/s10570-019-02262-x
Sadeghalvaad M, Dabiri E, Zahmatkesh S, Afsharimoghadam P (2019a) Improved curing conditions and mechanical/chemical properties of nitrile butadiene rubber composites reinforced with carbon based nanofillers. J Nanostruct 9:453–467. https://doi.org/10.22052/JNS.2019.03.007
Sadeghalvaad M, Dabiri E, Zahmatkesh S, Afsharimoghadam P (2019b) Preparation and properties evaluation of nitrile rubber nanocomposites reinforced with organo-clay, CaCO3, and SiO2 nanofillers. Polym Bull 76:3819–3839. https://doi.org/10.1007/s00289-018-2583-8
Sae-Oui P, Rakdee C, Thanmathorn P (2002) Use of rice husk ash as filler in natural rubber vulcanizates: In comparison with other commercial fillers. J Appl Polym Sci 83:2485–2493. https://doi.org/10.1002/app.10249
Sinclair A, Zhou X, Tangpong S et al (2019) High-Performance Styrene-Butadiene Rubber Nanocomposites Reinforced by Surface-Modified Cellulose Nano fibers. ACS Omega 4:13189–13199. https://doi.org/10.1021/acsomega.9b01313
Sombatsompop N, Thongsang S, Markpin T, Wimolmala E (2004) Fly ash particles and precipitated silica as fillers in rubbers. I. Untreated fillers in natural rubber and styrene-butadiene rubber compounds. J Appl Polym Sci 93:2119–2130. https://doi.org/10.1002/app.20693
Southern E, Thomas AG (1967) Diffusion of Liquids in Crosslinked Rubbers.Trans. Faraday Soc 63:1913–1921
Sreenath PR, Mandal S, Panigrahi H, Das P (2020) Fluorescence active, covalently conjugated and strong reinforcing nanofiller for polymer latex. Nano-Struct Nano-Objects 23:100477. https://doi.org/10.1016/j.nanoso.2020.100477
Sreenath PR, Singh S, Satyanarayana MS et al (2017) Carbon dot-unique reinforcing filler for polymer with special reference to physico-mechanical properties. Polymer 112:189–200. https://doi.org/10.1016/j.polymer.2017.02.014
Suryani E, Rashid A, Yehye WA et al (2017) Effect of Nanocellulose Loading on Tensile Properties of Nitrile Rubber. Solid State Phenom 264:112–115. https://doi.org/10.4028/www.scientific.net/SSP.264.112
Suzuki N, Ito M, Ono S (2005) Effects of rubber/filler interactions on the structural development and mechanical properties of NBR/silica composites. J Appl Polym Sci 95:74–81. https://doi.org/10.1002/app.20800
Taib MNAM, Yehye WA, Julkapli NM (2019) Influence of Crosslinking Density on Antioxidant Nanocellulose in Biodegradation and Mechanical Properties of Nitrile Rubber Composites. Fibers Polym 20:165–176. https://doi.org/10.1007/s12221-019-8575-y
Visakh PM, Monti M, Puglia D et al (2012a) Mechanical and thermal properties of crab chitin reinforced carboxylated SBR composites. Express Polym Lett 6:396–409. https://doi.org/10.3144/expresspolymlett.2012.42
Visakh PM, Thomas S, Oksman K, Mathew AP (2011) Cellulose nanofibres and cellulose nanowhiskers based natural rubber composites: Diffusion, sorption, and permeation of aromatic organic solvents. J Appl Polym Sci 124:1614–1623. https://doi.org/10.1002/app.35176 doi
Visakh PM, Thomas S, Oksman K, Mathew AP (2012b) Crosslinked natural rubber nanocomposites reinforced with cellulose whiskers isolated from bamboo waste: Processing and mechanical/thermal properties. Composites PartA 43:735–741. https://doi.org/10.1016/j.compositesa.2011.12.015
Vural S, Dikovics KB, Kalyon DM (2010) Cross-link density, viscoelasticity and swelling of hydrogels as affected by dispersion of multi-walled carbon nanotubes. Soft Matter 6:3870–3875. https://doi.org/10.1039/c0sm00099j
Wisittanawat U, Thanawan S, Amornsakchai T (2014) Mechanical properties of highly aligned short pineapple leaf fiber reinforced - Nitrile rubber composite: Effect of fiber content and Bonding Agent. Polym Test 35:20–27. https://doi.org/10.1016/j.polymertesting.2014.02.003
Zhao X, Hu H, Zhang D et al (2019) Curing behaviors, mechanical dynamic mechanical analysis and morphologies of natural rubber vulcanizates containing reclaimed rubber. e-Polymers 19:482–488
Ziegel ID, Romanov A (1973) Modulus Reinforcement in Elastomer Composites. I. Inorganic Fillers JAppl Polym Sci 17:1119–1131